Journal of Environmental Management 392 (2025) 126767

Contents lists available at ScienceDirect

Journal of Environmental Management

journal homepage: www.elsevier.com/locate/jenvman

Research article

Compost-based sustainable treatment for simulated textile dye effluents: Evaluating adsorption capacity and phytotoxicity

Iñaki Beceiro-Cillero [a], Juan Antelo [a], Pedro V. Verdes [b], Fátima Bento [c], Sarah Fiol [d,*]

[a] CRETUS, Department of Soil Science and Agricultural Chemistry, University of Santiago de Compostela, 15782, Santiago de Compostela, Spain
[b] Department of Applied Physics, University of Santiago de Compostela, 15782, Santiago de Compostela, Spain
[c] Department of Chemistry, Center of Chemistry, University of Minho, Campus Gualtar, Braga, 4710-057, Portugal
[d] CRETUS, Department of Physical Chemistry, University of Santiago de Compostela, 15782, Santiago de Compostela, Spain

ARTICLE INFO

Keywords:
Compost
cationic dye
Adsorption
Phytotoxicity
Decontamination
Valorization

ABSTRACT

Pollution from textile dye effluents is of growing environmental concern owing to the economic importance of the dye industry, the high toxicity of many dyes and the high cost of decontamination methods. This study evaluated urban-waste derived compost as an eco-friendly and cost-effective adsorbent to decontaminate simulated dye effluents. Batch adsorption experiments showed maximum adsorption capacities of 330, 150 and 35 mg g^{-1} for Crystal Violet (CV), Brilliant Green (BG), and Rhodamine B (RhB), respectively. Adsorption efficiencies exceeding 80–90 % were achieved under optimal pH and compost dosage. Fixed-bed column experiments confirmed the highest affinity for CV, with a breakthrough time of 700 min, compared to shorter times obtained for BG and RhB. The adsorption affinity largely depended on the chemical structure of the dye, as well as on compost functional groups and surface charge. Phytotoxicity assays using *Lollium perenne* revealed acute toxicity of CV and BG solutions, with germination rates below 30 % and marked root elongation inhibition. However, leachates from the dye-exposed compost had less effect on germination and root elongation than either non-dye-exposed compost leachates or pure dye solutions, suggesting that the dye-exposed compost poses minimal ecological risk. Overall, these findings confirm that urban-waste compost is an effective and viable adsorbent for textile dye removal from aqueous effluents, with strong potential for wastewater treatment applications and safe reuse as a soil amendment.

1. Introduction

Dyes are among the most commonly used and widely distributed chemical compounds, with such prominence in our lives that the dye industry has become one of the most economically important industries worldwide (Aqeel et al., 2020). Dyes have a key role in human activities, with a wide range of applications and an essential function in multiple industries. Traditionally, the dye industry relied on using natural compounds (pigments) with minimum environmental impact; however, synthetic dyes are now predominantly used because of their chromatic diversity, visual properties, stability and ease of synthesis (Aqeel et al., 2020; Al-Zawahreh et al., 2022; Przystaś et al., 2012). This transition has increased economic benefits and improved the quality and variety of products available. However, it has also led to significant environmental concerns. The environmental problems associated with the dye industry are derived from the strong dependence on freshwater, with an average consumption of 1.6 million litres of water per day per facility (Kant, 2011; Uddin, 2021). This leads to discharge of large amounts of dye effluent wastewater; e.g. reaching 217 m^3 in Bangladesh in 2016 (Uddin, 2021). The concentration of dye in wastewater may reach up to 7000 mg L^{-1} (typically ranging between 10 and 200 mg L^{-1} depending on the dyeing industry) and, if not properly treated, may jeopardise the quality of receiving water bodies and the health of the species and ecosystems that depend on them (Jorge et al., 2023; Yaseen and Scholz, 2019).

Triphenylmethane dyes are a group of chemical compounds characterized by the presence of at least one triphenylmethane group and strong chromatic intensity and brightness (Przystaś et al., 2012). Triphenylmethane dyes are widely used in the textile, paper and medical industries, as dyes, antiseptics and veterinary medicines (Al-Zawahreh et al., 2022). However, both the dyes and their derivates have been identified as highly toxic to bacteria, fungi, plants and animals. The toxicity can affect aquatic ecosystems directly, via mutagenic pathways,

* Corresponding author.
E-mail address: sarah.fiol@usc.es (S. Fiol).

https://doi.org/10.1016/j.jenvman.2025.126767
Received 14 April 2025; Received in revised form 14 July 2025; Accepted 26 July 2025
Available online 1 August 2025

or indirectly, by altering the light penetration in water bodies and affecting the photosynthetic and oxygenation rates in surface waters (Przystaś et al., 2012). Studies involving plants have shown that the mutagenic effects of these compounds can cause changes in the cell cycle and mitosis, triggering alterations in germination, root elongation and the rate of production of biogenic amines (Adomas et al., 2020; Bharagava et al., 2018; Mani and Bharagava, 2016; Vigneshpriya et al., 2019). Biomedical studies have also highlighted the high carcinogenic potential of these dyes and the low tolerance of humans to their effects, suggesting that both direct and indirect exposure should be avoided (Bharagava et al., 2018; Oplatowska et al., 2011). Triphenylmethane dyes are not the only dye compounds with potentially harmful effects on the biosphere. Other widely used dyes, such as rhodamines and other xanthene dyes, may exert the same direct and indirect effects as triphenylmethane dyes, in addition to damaging the photosynthetic apparatus and cell membranes and increasing oxidative stress in cells (Sharma et al., 2022; Skjolding et al., 2021; Sudarshan et al., 2022). Consequently, dyes such as rhodamines have been classified as mutagenic, oncogenic and neurotoxic, and additionally related to cutaneous, ocular, gastric and respiratory diseases (Sharma et al., 2022).

Multiple techniques have been developed for decontaminating dye industry effluents. Traditional approaches include using techniques such as ozonation, coagulation, flocculation, oxidation and reduction as primary methods for wastewater treatment (Przystaś et al., 2012). However, these techniques require highly specialized facilities and equipment, and as they target compound-dependent processes, their applicability is limited to resource-rich areas. Less expensive alternatives, such as biological degradation, have shown poor adaptability and limited application potential due to the diversity of pollutants involved. The most commonly used methods nowadays for depurating dye effluents are based on adsorption processes involving various materials. These can be synthetic (specifically created for their high efficiency, but expensive), semi-synthetic (produced by slight modifications of natural materials, with intermediate cost and efficiency) or waste materials (Al-Zawahreh et al., 2022). Natural materials and sub-products are of interest due to their potential efficiency for wastewater treatment, low cost and availability. Additionally, their environmental impact is often much lower than that of other adsorbents. Plant-derived products, such as sawdust and bark, are among the most used natural materials. For instance, the capacity of sawdust derived from trees of the genera *Pinus*, *Terminalia*, *Populus* and *Mansonia* to adsorb various dyes has been extensively tested, in studies involving azo (e.g. Direct Brown), triphenylmethane (e.g. Crystal Violet, Methyl Violet and Malachite Green) and phenothiazine dyes (e.g., Methylene Blue) (Ahmad, 2009; Dulman and Cucu-Man, 2009; Ofomaja, 2008; Pekkuz et al., 2008; Pimentel et al., 2023; Shakoor and Nasar, 2018; Witek-Krowiak, 2011). Similarly, bark from trees of *Eucalyptus*, *Pinus*, *Handroanthus* and *Ficus* genera has proven to be an effective sorbent for removing azo (e.g. Eriochrome black-T), anthraquinone (e.g. Alizarin Red), triphenylmethane (e.g. Crystal Violet) and phenothiazine dyes (e.g. Methylene Blue) from wastewater (Al-Zawahreh et al., 2022; Anastopoulos et al., 2022; Gul et al., 2022; Hernandes et al., 2019; Parvin et al., 2019; Saadallah et al., 2024; Sahmoune and Yeddou, 2016). Sewage sludge is also commonly used as a sorbent material and has shown to be effective for treating water contaminated with azo (e.g. Evans blue), triphenylmethane (e.g. Brilliant Green) and anthraquinone dyes (e.g. Vat Yellow 2, Red 10 and Orange 11) (Dhaouadi and M'Henni, 2009). More recently, compost has emerged as a promising natural material for treating dye effluents owing to its low cost, minimal environmental impact and potential to promote a circular economy, as it is derived from waste. Thus, several studies conducted using phenothiazine (e.g. Methylene Blue), xanthene (e.g. Basic Violet 10), azo (Acid Red 27, Acid Red 111, Basic Red 18, Direct Blue 151, Reactive Violet 4, Reactive Red 234 …) and compost-based sorbents have demonstrated the high dye removal efficiency and significant remediation potential of compost (Al-Zawahreh et al., 2021, 2024; McKay et al., 2011; Thillainayagam et al., 2023). However, few works have compared the adsorption behaviour of structurally diverse cationic dyes in both batch and continuous flow systems, relating the adsorption efficiency to compost surface charge and functional-group chemistry, or evaluated the phytotoxicity of dye-exposed compost to establish its potential safe reuse. Moreover, economic assessment of compost-based solutions remains scarce.

In the present study, we explored the potential of urban-waste compost as an eco-friendly, cost-effective sorbent material for the removal of synthetic dyes from aqueous effluents. We evaluated the capacity of composted organic waste to retain representative cationic dyes (Crystal Violet, Brilliant Green, and Rhodamine B) across varying pH, contact time and dye concentrations. Kinetic, equilibrium, and fixed-bed column experiments were conducted to evaluate the adsorption efficiency and to elucidate the adsorption mechanism, revealing that dye-compost interactions depend on both dye molecular structure and compost surface chemistry. We also assessed the toxicity of dye solutions and compost leachates by determining how they affect seed germination and root growth. The overall aim was to understand the valorization potential of compost from the selective collection of urban organic waste as a sustainable sorbent material for textile dye effluents, thereby promoting a more efficient and circular environmental management.

2. Materials and methods

Two industrially-produced composts derived from organic urban waste were tested: one was provided by the facilities of the Galician Environmental Society (SOGAMA) in Spain (hereafter SUW compost) and the other was produced by the Intermunicipal Waste Management Service of Greater Porto (LIPOR) in Portugal (hereafter PUW compost) and purchased under the commercial name Nutrimais. Before use, the compost samples were passed through a 2 mm sieve and washed with distilled water to remove soluble organic matter (Ramisio et al., 2023). The washing process involved shaking the compost suspensions on an end-over-end shaker for 3 h, at a solid:solution ratio of 1:500 (w:v), followed by centrifugation at 3000 rpm to separate the solid and aqueous phases. The supernatant was then discarded, and the solid sample was briefly washed again with distilled water and centrifuged for 10 min at 3000 rpm. This process was repeated until a colourless supernatant was obtained. Finally, the washed compost was dried at 45 °C in a preheated desiccation oven. Elemental analysis and general chemical characterization of the washed compost samples were conducted following the procedure described by Silva et al. (2022a); the results are summarised in Table 1. Compost samples were also characterized by ATR-FTIR spectroscopy using a JASCO FTIR 4200 spectrometer equipped with a ZnSe ATR crystal plate. FTIR spectra were recorded in transmission mode over a wavenumber range of 600–4000 cm^{-1}, with each spectrum representing the average of at least 50 co-added scans at a resolution of 1 cm^{-1}. The isoelectric point (IEP) was determined by titrating compost samples over a wide pH range, between 2 and 9, using a Malvern MPT-2 Multipurpose Titrator following a similar procedure to that described by Amini et al. (2020). Compost suspensions of 5 g L^{-1} in

Table 1
Chemical characteristics of the washed compost samples.

Parameter	SUW	PUW
pH	7.34	7.93
C (%)	39.58	32.90
$C_{oxidizable}$ (%)	37.56	29.3
N (%)	2.37	2.49
P_{total} (g kg^{-1})	14.1	4.7
Ca (g kg^{-1})	93.1	99.4
Mg (g kg^{-1})	2.6	5.0
Na (g kg^{-1})	4.8	9.0
K (g kg^{-1})	6.6	19.7
CEC (cmol (+) kg^{-1})	95.0	167.0

$NaNO_3$ 0.1M were titrated using 0.1 or 1M HNO_3 and KOH solutions. At each pH value, three measurements were taken, and the average electrophoretic mobility was calculated and converted to zeta potential using the Smoluchowski equation.

Dye sorption experiments were conducted simulating textile effluents using aqueous saline solutions of two triphenylmethane dyes and one xanthene dye (Fig. 1), all with industrial applications and high polluting potential: Brilliant Green or Basic Green 10 (BG), Rhodamine B or Basic Violet 10 (RhB) and Crystal Violet or Basic Violet 3 (CV). The solutions were prepared from 200 to 500 mg L^{-1} stock solutions, previously prepared in the laboratory from commercial powdered dyes. The dye concentrations selected for the sorption experiments are environmentally relevant, as they fall within the range reported for textile wastewater discharges (Yaseen and Scholz, 2019).

All chemicals were of Merck p.a. quality. A-grade glassware and polycarbonate material were used to prepare stock solutions and in the sorption experiments and bioassays. Double-distilled water was used in all of the experiments.

2.1. Batch experiments

2.1.1. Adsorption kinetics

To determine the adsorption kinetics of the dyes, aqueous solutions of 0.1 M $NaNO_3$ were prepared with varying concentrations of each dye at a pH between 5 and 6. The compost was suspended in the dye solutions at a concentration of 0.5 g L^{-1} (BG and CV) or 4 g L^{-1} (RhB). The following concentrations of dye were tested with both compost samples: 25, 50 and 80 (PUW) and 120 (SUW) mg L^{-1} for BG; 25 and 50 mg L^{-1} for RhB; and 50, 150 and 250 mg L^{-1} for CV. The suspensions were maintained by constant shaking (with the aid of a magnetic stirrer), at room temperature and in darkness. Aliquots of the suspensions were periodically removed for spectrophotometric analysis of the dye concentration in solution at wavelengths of 556, 590 or 625 nm (for CV, RhB and BG, respectively). Prior to analysis, the aliquots were centrifuged at 3000 rpm for 10 min, and the supernatant was retained for measurement. The concentration of sorbed dye was then calculated as the difference between the initial and final concentration of dye in solution.

Experimental data obtained from kinetic assays were, analysed using pseudo-first- and pseudo-second- order kinetic models (Arán et al., 2018; Pimentel et al., 2023).

- Pseudo-first-order kinetic model (PFO):

$$q_t = q_e\left(1 - e^{-k_1 t}\right) \quad \text{(Equation 1)}$$

- Pseudo-second-order kinetic model (PSO):

$$q_t = \frac{k_2 q_e^2 t}{(1 + q_e k_2 t)} \quad \text{(Equation 2)}$$

where t (min) is the reaction time, k_1 (min^{-1}) and k_2 (g mg^{-1} min^{-1}) are the sorption rate constants, and q_e and q_t (mg g^{-1}) represent the dye sorbed on the compost at equilibrium and at each time, respectively. Whereas PFO assumes a physisorption process, PSO assumes that the adsorption is proportional to the number of adsorption sites on the reactive surface and the rate of sorption is chemically controlled (López et al., 2019). The kinetic models were fitted to the experimental data by nonlinear regression analysis implemented with OriginPro 8 software.

2.1.2. Adsorption experiments

Adsorption isotherms, and pH and compost dose edges were obtained following the same procedure (Arán et al., 2018; Pimentel et al., 2023). In all experiments, the pH of the compost was adjusted prior to the experiments due to the buffering capacity of the compost samples. The compost suspensions were prepared in distilled water (maintaining the same solid:liquid ratio established for the subsequent experiments). After the pH was adjusted to the desired values using HNO_3 or NaOH at concentrations ranging from 0.01 to 1 M, the suspensions were equilibrated in an end-over-end shaker for 3 h at room temperature. The suspensions were then centrifuged at 3000 rpm for 10 min, after which the supernatant was discarded, and the solid compost was collected and used in the sorption experiments.

For the adsorption experiments, solid compost was resuspended in 25 mL of an aqueous solution containing dye and 0.1 M $NaNO_3$. The concentration of compost used to obtain the adsorption isotherms was 0.5 g L^{-1} for the BG and CV assays and 4 g L^{-1} for the RhB assays (because of the lower adsorption efficiency of RhB). Dye concentrations in aqueous solutions ranged from 0 to 200 mg L^{-1} for RhB assays, 0–140 mg L^{-1} for BG assays and 0–400 mg L^{-1} for CV assays. The pH was adjusted to 4 for practical and analytical convenience, using 0.01 or 0.1 M HCl or NaOH, and the suspensions were then placed in an end-over-end shaker for 24 h, at room temperature in darkness. The samples were then centrifuged at 3000 rpm for 10 min, and the solid was discarded. The supernatant was analysed spectrophotometrically to determine the concentration of dye in solution. The amount of dye retained by the compost was calculated as the difference between the initial and final concentrations of dye in solution. The adsorption isotherms were described using the Langmuir and Freundlich models (Arán et al., 2018; Pimentel et al., 2023).

- Langmuir model:

$$q_e = \frac{K_L \cdot Q_{max} \cdot C_e}{1 + K_L \cdot C_e} \quad \text{(Equation 3)}$$

- Freundlich model:

$$q_e = K_F \cdot C_e^{1/n} \quad \text{(Equation 4)}$$

where q_e is the concentration of dye sorbed on the compost (mg g^{-1}); C_e is the concentration of dye in solution (mg L^{-1}); K_L is the Langmuir

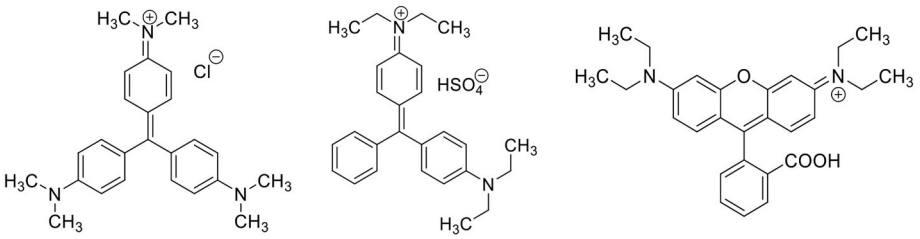

Fig. 1. Chemical structure of the dye molecules.

sorption constant, which is related to the affinity; and Q_{max} is the maximum sorption capacity of the compost (mg g^{-1}); K_F is the Freundlich constant related to the sorption capacity (mg g^{-1}) (L $mg^{-1})^{1/n}$; and n is a constant related to sorption intensity and binding sites heterogeneity. The Langmuir isotherm assumes a homogeneous sorbent surface with identical and energetically equivalent adsorption sites, whereas the Freundlich isotherm is a purely empirical model based on sorption to heterogeneous surfaces.

A similar procedure was followed in the pH edge experiments. In this case, the concentration of dye in aqueous solution was maintained at 50 mg L^{-1}, and the concentrations of compost were again 0.5 g L^{-1} for CV and BG assays and 4 g L^{-1} for RhB assays; the pH was varied between 3 and 8. To assess the effect of the amount of adsorbent on the adsorption rate, experiments were conducted using dye concentrations in aqueous solutions of 50 mg L^{-1} for all dyes, with the pH adjusted to 4 in all cases. Dye-specific amount of compost were used: 2–8 g L^{-1} for RhB, 0.25–4 g L^{-1} for BG and 0.1–2 g L^{-1} for CV.

2.1.3. Desorption experiments

To evaluate the desorption potential, aqueous solutions of 0.1 M $NaNO_3$ and 50 mg L^{-1} of the selected dye were prepared at pH 4, and 0.5 g L^{-1} (BG and CV) or 4 g L^{-1} (RhB) of compost (with pre-established pH treatment) were then suspended in the solutions. After adsorption equilibrium was reached (determined as noted above), the solid compost obtained after centrifugation was used in the desorption experiments.

In the desorption experiments, water (Sheppard and Thibault, 1992) and a 0.1 M KCl solution (modified from Li et al., 2020) were used to analyse the potential desorption under different extraction conditions. For desorption in water, dye-exposed compost suspensions in distilled water were prepared at a 1:20 solid:liquid ratio, and the pH was adjusted to values at which desorption was favoured (i.e. low adsorption; pH 5 for BG and CV, and pH 7 for RhB). The suspension was manually shaken and then held for 5 days at room temperature and in darkness. For desorption in KCl, dye-exposed compost suspensions in a 0.1 M KCl aqueous solution were prepared at a solid:liquid ratio of 1:5 (w:v). The suspension was mixed in an end-over-end shaker for 24 h at room temperature and in darkness. Suspensions from each experiment were then centrifuged for 10 min at 3000 rpm. The solid was discarded, and the supernatant was analysed spectrophotometrically at the corresponding wavelength to determine the dye concentration in solution and, consequently, the rate of desorption of dye from the compost.

2.2. Column experiments

Column adsorption experiments were conducted with a glass column (of internal diameter 15 mm and length 40 cm) coupled to automated pumping and effluent collection systems (Arán et al., 2017, 2018). The fixed-bed columns were filled with a 1 cm layer of perlite, and 0.5 or 2.5 g of SUW compost mixed with acid-washed quartz sand (particle size 0.25–0.30 mm) was added to a depth of 2 cm. This mixture was sandwiched between two layers of acid-washed quartz sand, 5 cm and 10 cm height, respectively. For the adsorption experiments, an aqueous solution of 0.01 M KCl and 15–20 mg L^{-1} of dye was passed through the column at a constant flow rate of 5 mL min^{-1}. Effluent samples were removed periodically for determination of both the pH and dye concentration, until the system reached saturation point or the available influent dye solution was exhausted.

The column assay results were described and analysed using the non-lineal Yan model, based on the Bohart-Adams model (Yan et al., 2001):

$$\frac{C}{C_0} = 1 - \frac{1}{1 + \left(\frac{C_0 \cdot F}{Q_{max} \cdot m_s} \cdot t\right)^a} \quad \text{(Equation 5)}$$

where C_0 (mg L^{-1}) is the dye concentration in the influent solution and C (mg L^{-1}) is the dye concentration in the effluent solution; F is the flow rate (L h^{-1}), a is an empirical parameter inversely related to the slope of the regression function, Q_{max} is the maximum sorption capacity of the compost (mg g^{-1}), m_s is the sorbent mass (g) and t is the run time (h). Model fitting was conducted using OriginPro 8.0 software, and errors in the parameters were minimized based on the residual sum of squares (RSS). The models derived from the Bohart–Adams model are used only to describe the experimental breakthrough curves, regardless of theoretical considerations (Arán et al., 2017).

2.3. Phytotoxicity experiments

The biological assays were conducted following the procedure described by Di Salvatore et al. (2008), using the ryegrass *Lollium perenne* as the model species. Ryegrass seeds were acquired from a commercial garden centre and sterilised by immersion in a 10 % sodium hypochlorite solution for 10 min. The seeds were then rinsed thoroughly with distilled water (to fully remove the sodium hypochlorite), air-dried and stored in darkness at room temperature.

For the assays, 20 seeds were evenly spaced on filter paper lining the bottom of a Petri dish (∅ = 11 cm). Three replicate Petri dishes were prepared for each treatment. Eight mL of the solution being tested was added to each Petri dish: i) control experiments were conducted by adding distilled water to the seeds; ii) leachates from washed compost were extracted with water or 0.1 M KCl for analysis the toxicity of compost leachates (following the procedure used in the desorption experiments); iii) aqueous solutions of each dye at concentrations 12.5, 25, 37.5 and 50 mg L^{-1} were used to define dye toxicity curves; and iv) dye-exposed compost leachates, extracted by both water and 0.1 M KCl (obtained from desorption experiments described in section 2.1.3).

After the addition of the test solution, the sealed Petri dishes containing the seeds were transferred to a germination chamber and maintained for 7 days at 22 °C in darkness (López et al., 2021; Rios et al., 2018). Finally, the seeds treated with the different solutions were collected to determine the germination rate (considering the germination threshold in root length ≥1 cm) and root elongation rates. The Relative Root Growth (%RRG) and Relative Seed Germination (%RSG) indices were used for this purpose (López et al., 2021):

$$\%RRG = \frac{\overline{L}_e}{\overline{L}_c} \cdot 100 \quad \text{(Equation 6)}$$

- Relative Root Growth:
- Relative Seed Germination:

$$\%RSG = \frac{\overline{G}_e}{\overline{G}_c} \cdot 100 \quad \text{(Equation 7)}$$

where $\overline{L}_e$ and $\overline{L}_c$ are the mean root length in the experiments and in the control, respectively, and $\overline{G}_e$ and $\overline{G}_c$ are the mean number of seeds germinated in the experiments and in the control, respectively.

Moreover, toxicity patterns and benchmarks (i.e. effective dose or ED) were also described for each dye, considering the results of seed germination and root elongation by graphic representation of the root elongation (cm) or seed germination (%) vs the concentration of aqueous dye solutions (mg L^{-1}). Thus, the thresholds ED_{25}, ED_{50} and ED_{75} were defined as the effective dye dose producing 25 %, 50 % and 75 % reduction, respectively, in seed germination or root elongation compared to the control.

3. Results

3.1. Compost characterization

The FTIR spectra of both compost samples (Fig. S1) exhibit

characteristic peaks of humified organic matter (Silva et al., 2022b; Smidt and Meissl, 2007), including: a band at 3320 cm^{-1}, ascribed to O-H stretching in alcohols, phenols or carboxyl groups; two bands at 2925 and 2845 cm^{-1}, attributed to show the characteristic the symmetric and asymmetric C-H stretching vibrations of CH_3 and CH_2 groups; a band centered around 1640–1630 cm^{-1}, assigned to aromatic C=C and C=O stretching of amide groups and quinonic C=O and/or C=O of H-bonded conjugated ketones; a band at 1540 cm^{-1}, corresponding to secondary amides; two bands between 1440 and 1420 cm^{-1}, associated with O-H deformation and C-O stretching in carboxylic groups, C-H deformations of CH_3 and CH_2 groups, and asymmetric stretching of COO- groups; a band around 1020 cm^{-1}, attributed to C-O stretching of polysaccharides, and Si-O bonds of silicate impurities; and finally a band at 870 cm^{-1} assigned to carbonates.

Fig. S2 shows the zeta potential curves of the compost samples within the pH range of 1–9 at two different compost dosages. All measured zeta potential values were negative throughout the entire pH range. As the experimental data points approach zero at low pH, the IEP can be estimated to be approximately 1.7 for SUW and below 1 for PUW.

3.2. Batch experiments

3.2.1. Adsorption kinetics

The dye adsorption kinetics on compost (Fig. 2 and Table 2) indicate that the equilibrium was reached faster at lower dye concentrations, independently of the dye or the compost. The increase in the equilibrium rate was, in all cases, directly related ($R^2 > 0.9$) to the concentration of the dye. For BG, equilibrium times were reached at 180–420 min with PUW and at 120–420 min with SUW and for CV at 100–420 min with both composts. For RhB, at 25 mg L^{-1}, the equilibrium was reached within 10 min (data were not recorded within this time). However, at higher concentrations equilibrium was reached after approximately 100 min with PUW and at 200 min with SUW. For all of the dyes (BG, RhB, CV), the kinetics can be described by either a PFO (Fig. 2, Table 2) or a PSO model (Fig. S3, Table S1). Both compost samples exhibited the same kinetic behaviour regardless of the nature of the dye. This was supported by the linear correlation (with a slope close to 1) between q_e values (calculated using PFO and PSO kinetic models) with PUW and SUW samples (Fig. S4). The equilibrium adsorption, q_e, expressed as mg of dye per gram of compost, followed the order CV > BG > RB.

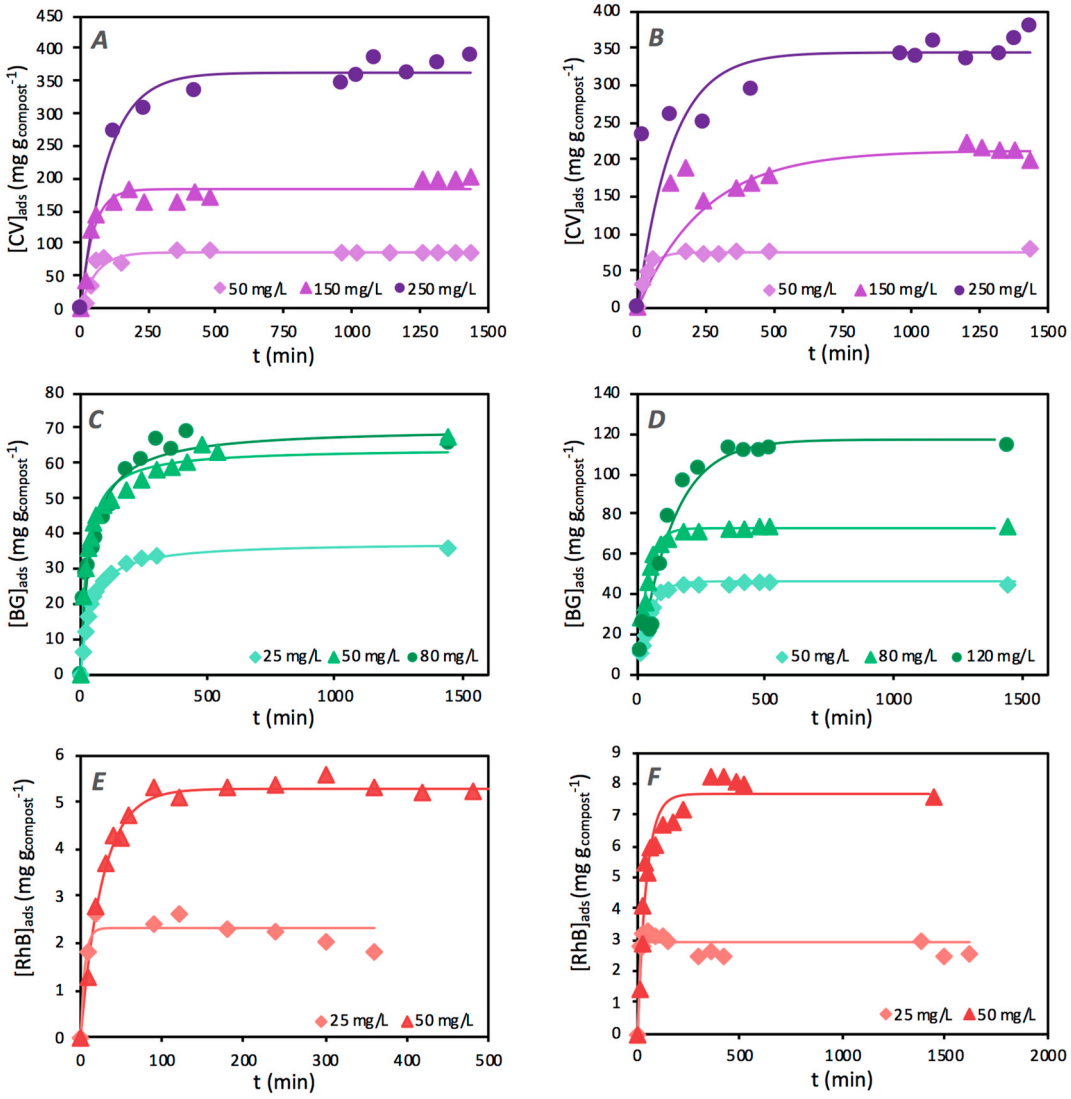

Fig. 2. Kinetics of dye adsorption on PUW (left) and SUW (right) compost samples at natural pH (5–6). Symbols represent the experimental results, and lines represent the Pseudo-First Order kinetic model. (A,B) CV; (C,D) BG; (E,F) RhB.

Table 2
Pseudo-first order kinetic model fitting parameters for adsorption of the dyes on compost samples.

Compost		[Dye] (mg L-1)	qe (mg g-1)	K1 (g min-1 mg-1)	R2
SUW	BG	50	46.0	2.2 × 10-2	0.992
		80	73.1	2.7 × 10-2	0.964
		120	116.9	7.5 × 10-3	0.966
	RhB	25	2.9	3.7 × 10-1	0.847
		50	7.7	2.4 × 10-2	0.945
	CV	50	74.2	2.7 × 10-2	0.974
		150	211.5	4.1 × 10-3	0.984
		250	344.0	8.0 × 10-3	0.925
PUW	BG	25	33.2	2.1 × 10-2	0.986
		50	58.7	2.8 × 10-2	0.921
		80	63.3	1.8 × 10-2	0.922
	RhB	25	2.3	1.9 × 10-1	0.879
		50	5.3	3.7 × 10-2	0.987
	CV	50	87.4	1.7 × 10-2	0.948
		150	185.3	2.2 × 10-2	0.934
		250	364.4	1.0 × 10-2	0.972

*p-value <0.05 Structured.

3.2.2. Adsorption experiments

Adsorption isotherms for the three dyes showed similar results for both composts (Fig. 3 and Fig. S5). For both composts, adsorption rates followed the same order as in the kinetics experiment: CV > BG > RhB. For CV, experimental adsorption reached values of 330 and 300 mg g^{-1} for SUW and PUW, respectively. For BG and RhB, the adsorption was significantly lower, with maximum adsorption capacities of approximately 150 and 35 mg g^{-1}, respectively. For all dyes, the adsorption was described using the Langmuir isotherm (Table 3), although for BG a slightly better fit was obtained using the Freundlich isotherm (Fig. S5 and Table S2).

The pH edge experiments clearly showed that pH influenced the adsorption of CV, BG and RhB, regardless of the compost sample (Fig. 4A and Fig. S6). For CV, the adsorption increased slightly with pH, from 75 mg g^{-1} at pH 3–90 mg g^{-1} at pH 7. For BG, adsorption followed a valley-shaped trend, with an adsorption minimum of 55 mg g^{-1} at pH 5; from there, it increased with pH, reaching a maximum of 95 mg g^{-1} at pH 8. By contrast, although the adsorption levels were lowest for RhB, adsorption decreased continuously as the pH increased, from 16 mg g^{-1} at pH 3–4 mg g^{-1} at pH 8.

Experiments studying the effect of the adsorbent dose revealed a relationship between compost concentration and the percentage of dye adsorbed, which depended on the nature of the dye. In this respect, for the same dye concentration, a concentration of compost above 0.1 g L^{-1} led to 100 % adsorption of CV, whereas for BG and RhB the same adsorption rate was achieved at concentrations of 2 and 6 g L^{-1}, respectively (Fig. 4B). This trend allows us to choose the optimal amount of adsorbent for each dye: 0.5 g L^{-1} for BG and CV and 4 g L^{-1} for RhB.

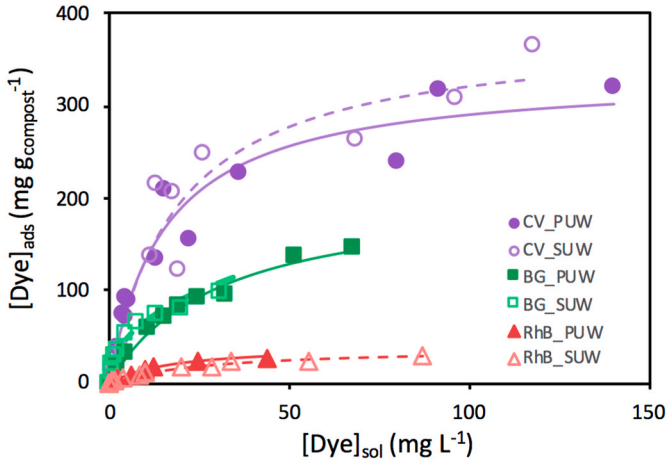

Fig. 3. Dye adsorption isotherms for the SUW (empty symbols) and PUW (full symbols) compost samples at pH 4.0. Symbols represent the experimental results, continuous lines represent the Freundlich isotherm and dashed lines represent the Langmuir isotherm. CV (circle); BG (square); RhB (triangle).

Table 3
Langmuir model fitting parameters for the adsorption of dyes on the compost samples.

Dye	Compost sample	Q_{max} (mg g^{-1})	K_L (L mg^{-1})	R^2
BG	SUW	124.81	0.157	0.939
	PUW	207.27	0.033	0.987
RhB	SUW	36.39	0.038	0.995
	PUW	37.65	0.060	0.991
CV	SUW	381.20	0.054	0.906
	PUW	333.40	0.066	0.952

*p-value <0.05.

3.2.3. Desorption experiments

Desorption assays revealed low desorption rates for all dyes, although the extraction method had distinct effects (Table S3). Only CV was detected in the water and KCl leachates in PUW, although the concentration measured was below 2 mg L^{-1}. The desorption rates for SUW were more variable. Although in most cases dye concentrations in the leachates were below 2 mg L^{-1} (desorption efficiencies generally under 5 %), the concentration of RhB in the water extract was much higher (8.27 mg L^{-1}), corresponding to a desorption efficiency of approximately 16.5 %.

3.3. Column experiments

The breakthrough curves obtained from the column assays are shown in Fig. 5. The time required by the effluent to reach the breakthrough (C_i/C_o = 0.05) and saturation points (C_i/C_o = 0.95) increased in the following sequence: RhB < BG < CV (Table S4). The breakthrough point also increased with the amount of compost in the column. This point was reached in less than 10 min for RhB, while it took more than 16 h to reach the same point for CV with 2.5 g of compost. For the fixed-bed columns filled with 0.5 g of compost, both the breakthrough and saturation points were reached in all cases. The breakthrough and saturation points occurred earliest for RhB, at 1 and 105 min, respectively. In contrast, these points were reached latest in the CV assays, at 75 and 525 min, respectively. For BG experiments, the breakthrough and saturation points occurred at 45 and 165 min. In the column experiments with 2.5 g of compost, breakthrough points were reached for all dyes, but in some cases saturation points occurred beyond the evaluated time range. Again, RhB exhibited the earliest breakthrough point, at 2 min, while the saturation point occurred after 309 min. The breakthrough point occurred latest in CV assays, at 690 min, with the saturation point found around 1350 min. In the case of BG, the breakthrough point occurred after 150 min, with the saturation point predicted to occur after 735 min.

All of the breakthrough curves were described by the Yan model. The maximum adsorption capacity, Q_{max}, varied in the order CV > BG > RhB (Table 4). This indicates that the increase in the compost sorption capacity was consistent with the results of the batch adsorption experiments.

3.4. Biotoxicity experiments

In the experiments conducted with aqueous dyes solutions, the dye concentration directly affected germination and root elongation, although each dye exhibited distinct behaviour (Fig. 6). In both panels (Fig. 6A and B), the thresholds for ED_{25}, ED_{50} and ED_{75} are indicated. Notably, the toxicity curves for BG (germination) and CV and RhB (root elongation) indicated that the reduction in germination and root

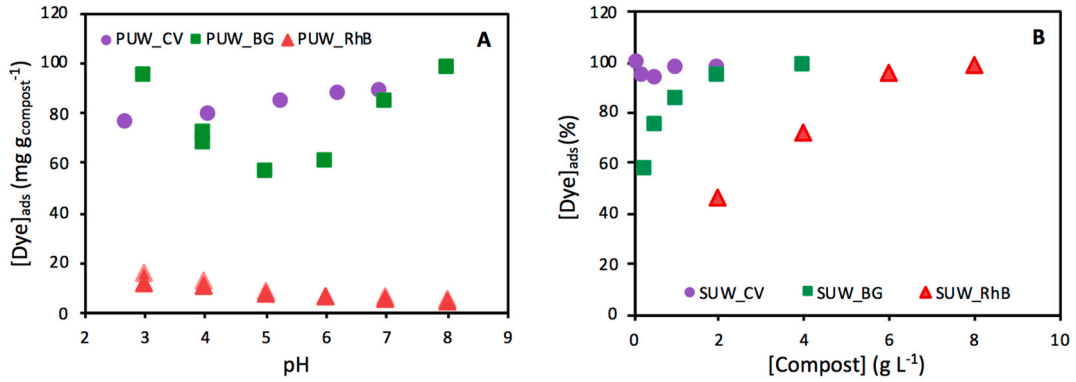

Fig. 4. (A) Effect of pH on adsorption of dyes on the PUW compost sample. (B) Effect of concentration of PUW on adsorption of the dyes at pH 4. Dye concentration of 50 mg L^{-1} was used in all experiments. CV (circle); BG (square); RhB (triangle).

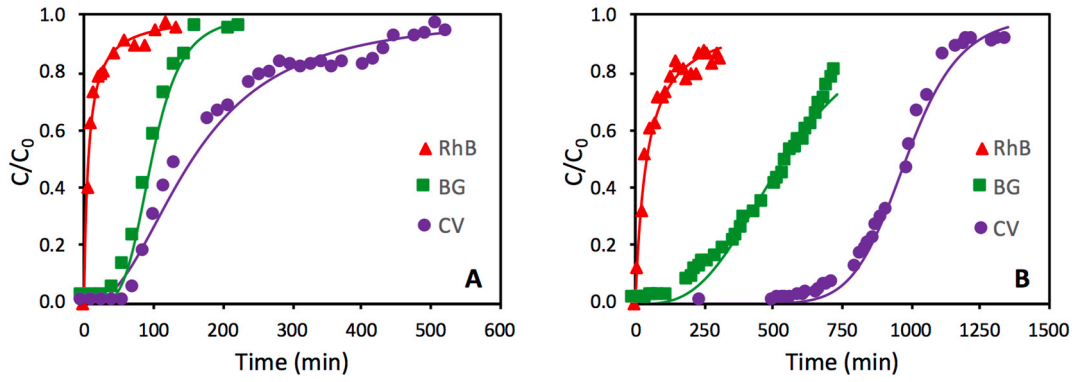

Fig. 5. Compost breakthrough curves for SUW with (A) 0.5 g and (B) 2.5 g of compost in the column at pH 5. Symbols correspond to the experimental results and lines to the Yan model fit. CV (circle); BG (square); RhB (triangle).

Table 4
Yan model fitting parameters for the breakthrough curves for adsorption of the dyes on SUW compost sample.

Dye	Compost (g)	a	Q_{max} (mg g^{-1})	R^2	RSS
BG	0.5	4.51	13.52	0.996	0.010
	2.5	3.12	14.13	0.982	0.043
RhB	0.5	1.02	1.42	0.991	0.008
	2.5	1.02	1.74	0.980	0.094
CV	0.5	2.31	31.08	0.983	0.059
	2.5	9.97	39.16	0.995	0.021

*p-value <0.05.

elongation rates was strongest at lower dye concentrations. For BG, germination decreased from 90 % to 17 % and 7.5 % in experiments at concentrations of 37.5 and 50 mg L^{-1}, respectively. The calculated ED_{50} for BG germination was 20.2 mg L^{-1}. Root elongation data are not shown for BG as the small number of germinated seeds hampers interpretation of the results. For RhB, although the germination rate was not affected, root length was significantly reduced, with a maximum decrease of approximately 50 %–60 % at concentrations above 25 mg L^{-1}. The ED_{50} for RhB producing root inhibition was estimated at 22.1 mg L^{-1}. In the case of CV, both germination and root elongation were affected by the dye concentration. Thus, the germination rate decreased from 90 % to 30 % as the concentration of CV increased, with the most pronounced decrease at higher concentrations of dye. The ED_{50} for CV on germination was observed at 42.5 mg L^{-1}. Regarding root elongation, reductions up to 60 % were obtained at 50 mg L^{-1}, with the most intense reduction occurring at lower concentrations of dye. The ED_{50} value for root inhibition was estimated at 13.7 mg L^{-1}.

The %RRG and %RSG for leachates of non-dye-exposed and dye-exposed composts are shown in Fig. 7. In the experiments conducted with leachates obtained from non-dye-exposed compost (black bars in Fig. 7), both compost samples produced similar results under the same washing conditions. Nevertheless, the inhibitory effect of the PUW leachate on the parameters evaluated (i.e. %RRG and %RSG) was less than that of the SUW leachate. Comparison of the extraction methods showed that the KCl-extracted leachates had a stronger inhibitory effect on germination and root elongation (i.e. lower rates) than the water-extracted leachates. Considering the experiments conducted with dye-exposed compost leachates, the results showed overall high germination and root elongation rates, most of which were similar to those obtained in the control experiments (coloured bars in Fig. 7). However, the results varied greatly depending on the treatment, especially for RhB and BG. In the case of BG, the average germination rates were higher for water-extracted leachates than for KCl-extracted leachates and also for PUW compost leachates than for SUW leachates. For RhB, while the PUW leachate yielded a slightly higher germination rate than the SUW leachate, neither the extraction method nor the compost sample used seem to follow any trend regarding the root elongation. The root lengths were longer for the water-extracted PUW and the KCl-extracted SUW leachate. Finally, for CV, the germination rates were only slightly affected by the extraction method, and experiments with KCl-extracted leachates revealed higher germination rates than those with water-extracted leachates.

4. Discussion

The study findings showed clear differences in both the removal efficiency and toxicity of each dye evaluated. According to the results of the batch experiments (kinetics, pH effect and isotherms), these

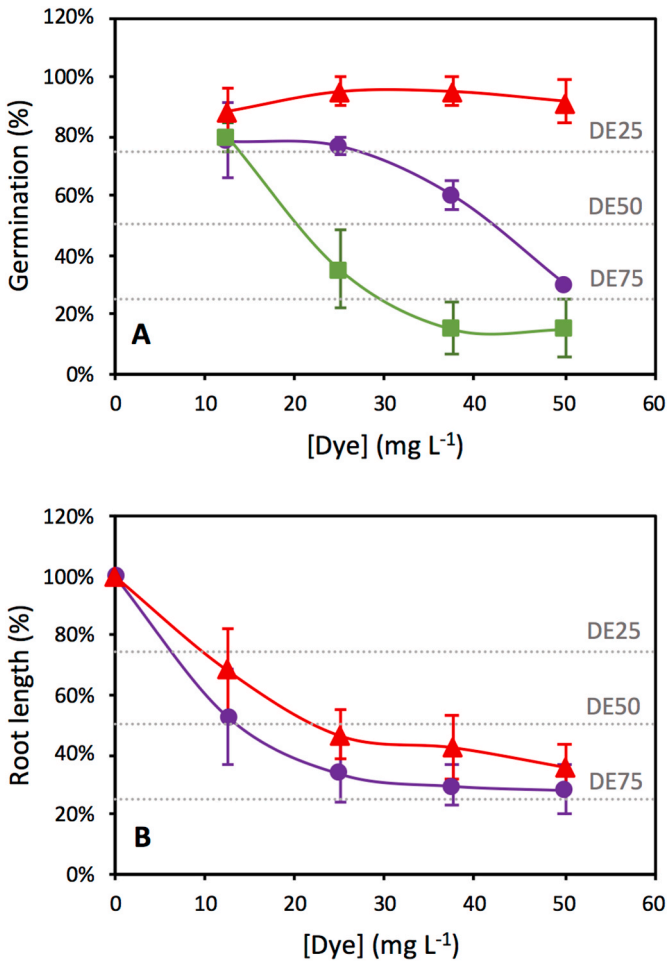

Fig. 6. (A) Germination and (B) Root length toxicity curves for aqueous solutions of dye and *Lollium perenne* seeds at dye concentration ranging from 12.5 to 50 mg L^{-1}. Symbols represent the experimental results (RhB: triangles, CV: circles, BG: squares), solid lines are for connecting experimental data points and dotted lines represent the effective doses ED_{25}, ED_{50} and ED_{75}.

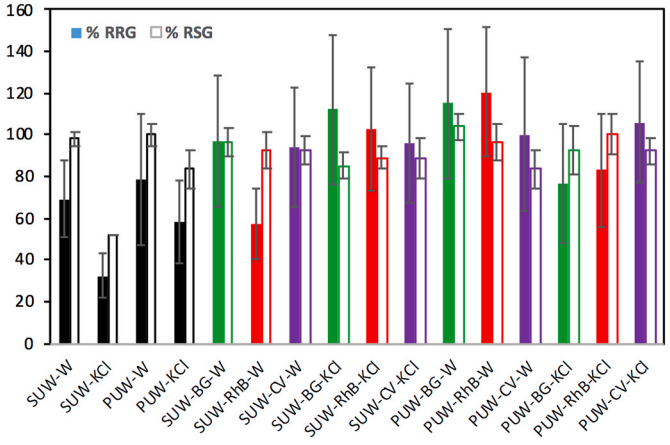

Fig. 7. Relative Root Growth (%RRG, filled bars) and Relative Seed Germination (%RSG, hollow bars) of *Lollium perenne* seeds obtained in the different experimental treatments. Non-dye-exposed composts (black bars), Brilliant Green (green bars), Rhodamine B (red bars) and Crystal Violet (purple bars) and for SUW and PUW compost samples are shown. Initial dye concentration in the sorption cycle was 50 mg L^{-1}. Values above 100 % are derived from the comparison with the control (distilled water).

differences cannot be attributed to the compost sample used, probably because both composts have the same origin (organic urban waste) and similar chemical composition (Table 1) although collected and processed in two different countries. Regarding adsorption, the batch and column experiments showed the highest removal efficiency for CV, followed by BG and RhB. These differences can be attributed to the inherent chemical nature and structure of the dyes (Fig. 1), particularly their cationic and basic nature, which facilitates adsorption reactions with compost (Pekkuz et al., 2008). Thus, the lower sorption values obtained for RhB than for BG and CV may be associated with the planar structure and the presence of carboxylic groups, which can hinder the electrostatic interactions and ion-dipole forces between the positively charged amine group of the dye and the main anionic functional groups present in the compost through electrostatic and steric effects (Fan et al., 2020; Putri et al., 2020; Sánchez-Martín et al., 2011). Moreover, the effects may also be explained by differences in the number of amine groups in each dye (which determine the ability to form hydrogen bonds), the degree of substitution of amine radicals (linked to the basic nature of the dyes and their affinity for the sorbent), the type of substituent radicals in the amine group (ethyl or methyl) and the steric hindrance of the positively charged amine group by the ethyl radicals (Putri et al., 2020; Al-Shehri et al., 2021; Dhodapkar et al., 2007). These factors explain the dye-dependent differences observed in the batch adsorption experiments. In the adsorption kinetic study, q_e increased in the order CV > BG > RhB, while k_1 increased in the opposite order. In the isotherms, the maximum adsorption, Q_{max}, at pH 4 followed the same order. As previously indicated, adsorption of the dyes on the compost is better described by the Langmuir equation, which is consistent with the formation of a monolayer on a homogeneous surface with uniform binding sites. In this regard, there is no consensus regarding whether dye adsorption preferably follows the Langmuir or Freundlich model (Nahali et al., 2022). The small difference found between Langmuir and Freundlich fittings (Fig. S5) suggests that the adsorption behaviour might be intermediate, following a Freundlich-like behaviour at low dye concentrations and approaching Langmuir-type monolayer saturation at higher concentrations. Similarly, the results of column experiments indicated the same trend, with RhB reaching saturation and breakthrough points faster, followed by BG and finally by CV. Nevertheless, variations in flow rate, fixed-bed height or total amount of sorbent material can affect the adsorption efficiency of fixed-column systems (Arán et al., 2017; Arán et al., 2018; Al-Zawahreh et al., 2022). In particular, decreasing the flow rate in the fixed-bed column system tends to increase the saturation and breakthrough times. The differences observed among the three dyes are difficult to compare with other adsorption data available in the literature. No studies have been found in which adsorption tests were conducted with the three dyes on the same material. Maximum adsorption capacity values have been found in materials of similar origin; however, the differences vary depending on whether the materials were subjected to a prior treatment or activation process or whether the material comes from the shell or the seed of a particular species (Nahali et al., 2022; Kumaravel et al., 2024; Kosale et al., 2024; Saeed et al., 2010). Literature data report maximum adsorption capacities ranging from 10 to 250 mg g^{-1}, 30–500 mg g^{-1} or 20–600 mg g^{-1}, for BG, RhB and CV, respectively, on activated carbons and biochar (Table S5). Given the wide variety of adsorbent materials reported, establishing a direct connection between the nature of the adsorbent and the observed behaviour remains challenging. Moreover, to evaluate the suitability of these materials in dye removal, it is necessary to consider not only their adsorption capacity but also the estimated cost associated with the removal process (Table S5).

For CV, studies with other sorbent materials showed similar pH-related changes, i.e. adsorption of CV increasing with increasing pH of the system (Al-Shehri et al., 2021; Kosale et al., 2024; Saeed et al., 2010). As a cationic dye, CV carries a positive charge, while the compost surface is negatively charged. As shown in Fig. S2, compost becomes

more negatively charged as the pH increases, and the electrostatic interactions between compost and CV are thus more favourable and adsorption is promoted at higher pH values. Cationic exchange between CV and the sorbent surface may be an important factor in the removal of this molecule at relatively high pH, at which the concentration of protons is low (Saeed et al., 2010). The experimental data showed a valley-shaped curve for BG adsorption as a function of pH with a clear increase in adsorption as the pH goes from 5 to 8. This behaviour can be explained in the same way as for CV, as both are cationic dyes with similar structure. In the curve, adsorption was minimal at pH 5, which is consistent with the pK_a of BG, 4.93 (Castro Silva et al., 2016). BG is fully protonated below this point, thereby increasing the interaction with the negatively charged surface of the compost, whose IEP is below pH 2 in both samples (Fig. S2). However, different trends have been reported in describing the effect of pH on BG adsorption (Nandi et al., 2009; Paul et al., 2024; Vyavahare et al., 2021). Some studies reported peak adsorption values, with the maximum varying significantly depending on the sorbent material (pH 5 for activated carbon from corn cob (Kumaravel et al., 2024); pH 8 for a ternary nanocomposite (Katowah and Alzahrani, 2023), and various explanations were provided to explain the different behaviour. A slight increase in adsorption as the pH increases has been also described for fava bean peels (Nahali et al., 2022), which was mainly justified by the PZC of the sorbent material. The RhB adsorption followed the expected trend in relation to pH, with removal efficiency decreasing as the pH increased. This is a consequence of the increase in negatively charged groups on both the adsorbate and sorbent, hindering the sorption process. RhB changes from cationic to zwitterionic form above pH 4.2 due to the deprotonation of the aromatic carboxylic groups (Yu et al., 2013), while the compost surface becomes increasingly negatively charged above pH 2 (Fig. S2). Adsorption rates vary at each pH value relative to those described for more homogeneous adsorbents and depend on the chemical composition of the compost. These differences may be explained by the more variable composition of compost than of other sorbents, which leads to a more complex chemical response to pH changes due to the highly diverse reactive sites. FTIR results (Fig. S1) suggest the presence of reactive carboxylic and phenolic groups, as well as amides and aromatic structures, which may be involved in interactions with the organic dyes. Thus, hydrogen bonds are expected to form between the oxygen-containing functional groups in compost and the nitrogen present in the dye molecular structure (Fig. 1). Moreover, π- π interactions can occur between the aromatic rings of the dyes and the aromatic structures present in the compost. Also, the previous analysis of the pH effect on the sorption capacity and the actual IEP of compost, confirmed the existence of electrostatic attraction/repulsion depending on the nature of the dye.

The amount of sorbent also affected the capacity of the compost to adsorb RhB, BG and CV. The responses of all dyes were consistent with those reported in previous studies (Nahali et al., 2022; Kumaravel et al., 2024; Kosale et al., 2024; Saeed et al., 2010), with greater adsorption at higher concentrations of sorbent. Increasing the concentration of compost provides more active sites, thus enhancing the dye removal. Considering the different affinities of the three dyes for the compost (CV > BG > RhB), larger doses of compost were needed to achieve 100 % adsorption following the same order. The investigation of pH and compost dosage as key operational parameters in dye adsorption processes demonstrated that an appropriate combination of these conditions can result in removal efficiencies ranging from 80 to 97 %.

The phytotoxicity of dye solutions was assessed through dose–response analysis using *Lolium perenne* germination as a bioindicator. The results indicate that all three dyes exhibit significant toxicity, as evidenced by the inhibition of seed germination and root elongation upon exposure to dye solutions. The severity of the response varies depending on the chemical nature of the dye. Triphenylmethane dyes (BG, CV), in particular, caused complete inhibition of germination, suggesting a high level of phytotoxicity. In contrast, the xanthene dye (RhB) did not affect germination but did impair root growth. The overall effects on germination and root elongation from dye-exposed compost leachates were more positive (i.e. higher germination and root elongation rates) than predicted by toxicity curves for the same dye concentration (50 mg L^{-1}). This can be explained by the results of desorption and biological assays, which showed a low desorption rate and low toxicity of the dye-exposed compost leachates, suggesting the potential safety of reusing the compost as a fertilizer. Desorption rates for all dyes and extractants were consistently low (<2 mg L^{-1}), with the only exception of the RhB-exposed compost in the water-extracted leachates, in which desorption reached values close to 8 mg L^{-1}. This may be attributed to the pH of the extraction medium (pH > 6) due to the basic character of the compost, as suggested by the lower adsorption rates observed for RhB at higher pH (Fig. 4A). This could be easily resolved by controlling the pH during the compost application, as desorption rates were lower at lower pH. Nevertheless, in all cases desorption rates were well below the corresponding 25 % effective dose (ED_{25}) obtained from germination toxicity curves (Fig. 6), which varied from 14 to 27 mg L^{-1} for BG and CV, respectively. For Rhb, the 25 % ED was not reached at any dye concentration. The minimal dye desorption and its effects are attenuated by the dye-compost interaction, thereby reducing the expected toxicity and supporting reuse of the compost.

An important advantage of using compost as an adsorbent lies in its low cost, especially when compared to conventional or alternative adsorbents, such as activated carbon or biochar. Compost can be locally produced from agricultural or urban organic waste, significantly reducing both material and transport costs. Previous studies have estimated compost production cost to range between $15-$70 per ton, depending on the feedstock and processing method (Torrijos et al., 2021), whereas the cost of activated carbon ranges from $1200 to $1800 per ton, and biochar from $485 to $600 per ton (León et al., 2020; Campion et al., 2023). This makes compost a highly accessible material for large-scale or decentralized applications in wastewater treatment (Table S5). Additionally, the potential to reuse dye-exposed compost as soil amendment adds further value, reinforcing its alignment with circular economy and sustainability principles. However, further studies assessing the full economic feasibility, including production, operation and regeneration costs, are still required.

5. Conclusions

This study demonstrates that compost derived from urban organic waste is a highly effective, low-cost adsorbent for cationic dyes in aqueous solutions. Under equilibrium conditions, maximum adsorption capacities reached 330 mg g^{-1} for CV, 150 mg g^{-1} for BG, and 35 mg g^{-1} for RhB, with removal efficiencies of 80–97 % under optimal pH and compost doses. The varying affinity, CV > BG > RhB, and the adsorption pH dependence reflect differences in the dye molecular structure and compost surface chemistry. The presence of oxygen- and nitrogen-containing functional groups (carboxyl, phenol, amides) in compost, and its net negative surface charge, IEP <2, promote electrostatic attraction/repulsion, hydrogen bonding, and π−π interactions. Adsorption behaviour is well described by both Langmuir and Freundlich isotherms, confirming the heterogeneous nature of dye interactions with compost. The fixed-bed column experiments further validate the efficiency of compost, as evidenced by extended breakthrough and saturation times for CV, followed by BG and RhB. The increased breakthrough time with higher doses of compost indicates the potential scalability and adaptability of effluent treatment. Desorption tests revealed minimal dye leaching, varying between 0.11 for BG and 8.27 mg L^{-1} for RhB, which can be further reduced via pH control to ensure minimal environmental compost. Finally, the phytotoxicity assays with *Lollium perenne* showed that, although the dye solutions had strong adverse effects, leachates from dye-exposed compost exhibited low toxicity, supporting the potential reuse of the composts as soil amendments. Overall, urban-waste compost provides high removal efficiency, selectivity, and reusability at low cost, aligning with circular-economy

principles and offering an eco-friendly alternative to conventional adsorbents.

CRediT authorship contribution statement

Iñaki Beceiro-Cillero: Writing – original draft, Methodology, Investigation, Formal analysis, Data curation. **Juan Antelo:** Writing – review & editing, Methodology, Investigation, Data curation, Conceptualization. **Pedro V. Verdes:** Writing – review & editing, Methodology, Investigation. **Fátima Bento:** Writing – review & editing, Validation, Resources, Funding acquisition, Conceptualization. **Sarah Fiol:** Writing – review & editing, Resources, Project administration, Methodology, Funding acquisition, Conceptualization.

Declaration of generative AI and AI-assisted technologies in the writing process

During the preparation of this work the authors used ChatGPT for assistance with refining language and improving the clarity of the manuscript. After using this tool, the authors reviewed and edited the content as needed and take full responsibility for the content of the publication.

Declaration of competing interest

The authors declare that they have no known competing financial interests or personal relationships that could have appeared to influence the work reported in this paper.

Acknowledgments

This work was financially supported by the VA Spain-Portugal Programme (EU) through the project Res4Valor (0791_RES4VALOR_1_E). I. Beceiro-Cillero, J. Antelo, and S. Fiol, belong to the Cross-disciplinary Research in Environmental Technologies (CRETUS) Research Center, ED431G 2023/12) and were also supported by the Group of Excelence GI-1245 financed by the Xunta de Galicia (ED431C 2022/40). I. Beceiro-Cillero is grateful to the Spanish Ministerio de Ciencia, Innovación y Universidades for grant awarded within the Programa de Formación de Profesorado Universitario (FPU 2023, grant number: FPU23/02836). The authors thank M. Santiso and F. Casas for their assistance in the characterization of the compost samples. The authors thank the Galician Environmental Society (SOGAMA) for the supply of compost samples.

Appendix A. Supplementary data

Supplementary data to this article can be found online at https://doi.org/10.1016/j.jenvman.2025.126767.

Data availability

Data are available through Mendeley Data at: Mendeley Data, V2, doi: 10.17632/rxmfy2sf72.2.

References

Adomas, B., Sikorski, Ł., Bęś, A., Warmiński, K., 2020. Exposure of *Lemna minor* L. to gentian violet or Congo red is associated with changes in the biosynthesis pathway of biogenic amines. Chemosphere 254, 126752. https://doi.org/10.1016/j.chemosphere.2020.126752.

Ahmad, R., 2009. Studies on adsorption of crystal violet dye from aqueous solution onto coniferous pinus bark powder (CPBP). J. Hazard Mater. 171, 767–773. https://doi.org/10.1016/j.jhazmat.2009.06.060.

Al-Shehri, H.S., Almudaifer, E., Alorabi, A.Q., Alanazi, H.S., Alkorbi, A.S., Alharthi, F.A., 2021. Effective adsorption of crystal violet from aqueous solutions with effective adsorbent: equilibrium, mechanism studies and modeling analysis. Environ. Pollut. Bioavailab. 33, 214–226. https://doi.org/10.1080/26395940.2021.1960199.

Al-Zawahreh, K., Barral, M.T., Al-Degs, Y., Paradelo, R., 2021. Comparison of the sorption capacity of basic, acid, direct and reactive dyes by compost in batch conditions. J. Environ. Manag. 294, 113005. https://doi.org/10.1016/j.jenvman.2021.113005.

Al-Zawahreh, K., Barral, M.T., Al-Degs, Y., Paradelo, R., 2022. Competitive removal of textile dyes from solution by pine bark-compost in batch and fixed bed column experiments. Environ. Technol. Innov. 27, 102421. https://doi.org/10.1016/j.eti.2022.102421.

Al-Zawahreh, K., Barral, M.T., Paradelo, R., 2024. Assessment of batch and fixed bed processes for competitive removal of direct dyes by a grade III compost adsorbent: relative efficacy factor. Water Air Soil Pollut. 235, 604. https://doi.org/10.1007/s11270-024-07419-4.

Amini, M., Antelo, J., Fiol, S., Rahnemaie, R., 2020. Modeling the effects of humic acid and anoxic condition on phosphate adsorption onto goethite. Chemosphere 253, 126691. https://doi.org/10.1016/j.chemosphere.2020.126691.

Anastopoulos, I., Ahmed, M.J., Hummadi, E.H., 2022. *Eucalyptus*-based materials as adsorbents for heavy metals and dyes removal from (waste)waters. J. Mol. Liq. 356, 118864. https://doi.org/10.1016/j.molliq.2022.118864.

Aqeel, K., Mubarak, H.A., Amoako-Attah, J., Abdul-Rahaim, L.A., Khaddar, R.A., Abdellatif, M., et al., 2020. Electrochemical removal of brilliant green dye from wastewater. IOP Conf. Ser. Mater. Sci. Eng. 888, 012036. https://doi.org/10.1088/1757-899X/888/1/012036.

Arán, D., Antelo, J., Lodeiro, P., Macías, F., Fiol, S., 2017. Use of waste-derived biochar to remove copper from aqueous solution in a continuous-flow system. Ind. Eng. Chem. Res. 56, 12755–12762. https://doi.org/10.1021/acs.iecr.7b03056.

Arán, D., Antelo, J., Fiol, S., Macías, F., 2018. Immobilization of phosphate by a technosol spolic silandic: kinetics, equilibrium and dependency of environmental variables. J. Soils Sediments 18, 2914–2923. https://doi.org/10.1007/s11368-018-1970-y.

Bharagava, R.N., Mani, S., Mulla, S.I., Saratale, G.D., 2018. Degradation and decolourization potential of an ligninolytic enzyme producing *Aeromonas hydrophila* for crystal violet dye and its phytotoxicity evaluation. Ecotoxicol. Environ. Saf. 156, 166–175. https://doi.org/10.1016/j.ecoenv.2018.03.012.

Campion, L., Bekchanova, M., Malina, R., Kuppes, T., 2023. The costs and benefits of biochar production and use: a systematic review. J. Clean. Prod. 408, 137138. https://doi.org/10.1016/j.jclepro.2023.137138.

Castro Silva, F., Fernandes da Silva, M.M., Brandao Lima, L.C., Anteveli Osajima, J., Silva Filho, C., 2016. Integrating chloroethyl phosphate with biopolymer cellulose and assessing their potenetial for adsorbing brilliant green dye. J. Environ. Chem. Eng. 4, 3348–3356. https://doi.org/10.1016/j.jece.2016.07.010.

Dhaouadi, H., M'Henni, F., 2009. Vat dye sorption onto crude dehydrated sewage sludge. J. Hazard Mater. 164, 448–458. https://doi.org/10.1016/j.jhazmat.2008.08.029.

Dhodapkar, R., Rao, N.N., Pande, S.P., Nandy, T., Devotta, S., 2007. Adsorption of cationic dyes on jalshakti®, super absorbent polymer and photocatalytic regeneration of the adsorbent. React. Funct. Polym. 67, 540–548. https://doi.org/10.1016/j.reactfunctpolym.2007.03.007.

Di Salvatore, M., Carafa, A.M., Carratù, G., 2008. Assessment of heavy metals phytotoxicity using seed germination and root elongation tests: a comparison of two growth substrates. Chemosphere 73, 1461–1464. https://doi.org/10.1016/j.chemosphere.2008.07.061.

Dulman, V., Cucu-Man, S.M., 2009. Sorption of some textile dyes by beech wood sawdust. J. Hazard Mater. 162, 1457–1464. https://doi.org/10.1016/j.jhazmat.2008.06.046.

Fan, H., Ma, Y., Wan, J., Wang, Y., 2020. Removal of gentian violet and rhodamine B using banyan aerial roots after modification and mechanism studies of differential adsorption behaviors. Environ. Sci. Pollut. Res. 27, 9152–9166. https://doi.org/10.1007/s11356-019-07024-7.

Gul, A., Muhammad, S., Nawaz, S., Munir, S., Rehman, K.U., Ahmad, S., et al., 2022. *Ficus religiosa* bark an efficient adsorbent for Alizarin Red S dye: equilibrium and kinetic analysis. J. Iran. Chem. Soc. 19, 1737–1746. https://doi.org/10.1007/s13738-021-02413-7.

Hernandes, P.T., Oliveira, M.L.S., Georgin, J., Franco, D.S.P., Allasia, D., Dotto, G.L., 2019. Adsorptive decontamination of wastewater containing methylene blue dye using golden trumpet tree bark (*Handroanthus albus*). Environ. Sci. Pollut. Res. 26, 31924–31933. https://doi.org/10.1007/s11356-019-06353-x.

Jorge, A.M.S., Athira, K.K., Alves, M.B., Gardas, R.L., Pereira, J.F.B., 2023. Textile dyes effluents: a current scenario and the use of aqueous biphasic systems for the recovery of dyes. J. Water Process Eng. 55, 104125. https://doi.org/10.1016/j.jwpe.2023.104125.

Kant, R., 2011. Textile dyeing industry an environmental hazard. Nat. Sci. 4, 22–26. https://doi.org/10.4236/ns.2012.41004.

Katowah, D.F., Alzahrani, H.K., 2023. A new ternary nanocomposites-based cellulose derivatives-$CuFe_2O_4$-zeolite with ultra-high adsorption capacity for Brilliant Green dye treatment and removal from the aquatic environment. J. Saudi Chem. Soc. 27, 101764. https://doi.org/10.1016/j.jscs.2023.101764.

Kosale, D., Singh, V.K., Thakur, C., 2024. Comparative adsorption of cationic and anionic dye by using non-activated Black Plum seed and biochar for aquatic phase: isotherm, kinetic and thermodynamic studies. Ind. Crop. Prod. 215, 118609. https://doi.org/10.1016/j.indcrop.2024.118609.

Kumaravel, S., Geetha, M., Niyitanga, T., Senthil Kumar, D., Al-Ansari, M.M., Mythili, R., et al., 2024. Preparation and characterization of activated carbon from corn cob by chemical activation and their adsorption of brilliant green dye from wastewater. Process Saf. Environ. Prot. 188, 1338–1345. https://doi.org/10.1016/j.psep.2024.05.127.

León, M., Silva, J., Carrasco, S., Barriento, N., 2020. Design, Cost estimation and sensitivity analysis for a production process of activated carbon from waste nutshells by physical activation. Processes 8, 945. https://doi.org/10.3390/pr8080945.

Li, Y., Wang, T., Camps-Arbestain, M., Suárez-Abelenda, M., Whitby, C.P., 2020. Lime And/or phosphate application affects the stability of soil organic carbon: evidence from changes in quantity and chemistry of the soil water-extractable organic matter. Environ. Sci. Technol. 54, 13908–13916. https://doi.org/10.1021/acs.est.0c01341.

López, R., Antelo, J., Fiol, S., Macías-García, F., 2019. Phosphate adsorption on an industrial residue and subsequent use as an amendment for phosphorous deficient soils. J. Clean. Prod. 230, 844–853. https://doi.org/10.1016/j.jclepro.2019.05.092.

López, R., Antelo, J., Silva, A.C., Bento, F., Fiol, S., 2021. Factors that affect physicochemical and acid-base properties of compost and vermicompost and its potential use as a soil amendment. J. Environ. Manag. 300, 113702. https://doi.org/10.1016/j.jenvman.2021.113702.

Mani, S., Bharagava, R.N., 2016. Exposure to crystal violet, its toxic, genotoxic and carcinogenic effects on environment and its degradation and detoxification for environmental safety. In: de Voogt, W.P. (Ed.), Reviews of Environmental Contamination and Toxicology. Springer, New York, pp. 71–104. https://doi.org/10.1007/978-3-319-23573-8_4.

McKay, G., Hadi, M., Samadi, M.T., Rahmani, A.R., Aminabad, M.S., Nazemi, F., 2011. Adsorption of reactive dye from aqueous solutions by compost. Desalination Water Treat. 28, 164–173. https://doi.org/10.5004/dwt.2011.2216.

Nahali, L., Miyah, Y., Mejbar, F., Benjelloun, M., Assila, O., Fahoul, Y., et al., 2022. Assessment of brilliant green and eriochrome black T dyes adsorption onto fava bean peels: kinetics, isotherms and regeneration study. Desalination Water Treat. 245, 255–269. https://doi.org/10.5004/dwt.2022.27945.

Nandi, B.K., Goswami, A., Purkait, M.K., 2009. Adsorption characteristics of brilliant green dye on kaolin. J. Hazard Mater. 161, 387–395. https://doi.org/10.1016/j.jhazmat.2008.03.110.

Ofomaja, A.E., 2008. Kinetic study and sorption mechanism of methylene blue and methyl violet onto mansonia (*Mansonia altissima*) wood sawdust. Chem. Eng. J. 143, 85–95. https://doi.org/10.1016/j.cej.2007.12.019.

Oplatowska, M., Donnelly, R.F., Majithiya, R.J., Glenn Kennedy, D., Elliott, C.T., 2011. The potential for human exposure, direct and indirect, to the suspected carcinogenic triphenylmethane dye brilliant green from green paper towels. Food Chem. Toxicol. 49, 1870–1876. https://doi.org/10.1016/j.fct.2011.05.005.

Parvin, S., Wasikur Rahman, M.D., Saha, I., Alam, M.D., Khan, M., 2019. Coconut tree bark as a potential low-cost adsorbent for the removal of methylene blue from wastewater. Desalination Water Treat. 146, 385–392. https://doi.org/10.5004/dwt.2019.23598.

Paul, A.S., Khan, S.H., Hasan, I., Siddiqui, S., 2024. Preparation and performance of novel bio-nanocomposite ZnMg@PH for the removal of hazardous brilliant green, crystal violet, and diclofenac sodium. Biomass Conv Bioref. https://doi.org/10.1007/s13399-024-05801-0.

Pekkuz, H., Uzun, I., Güzel, F., 2008. Kinetics and thermodynamics of the adsorption of some dyestuffs from aqueous solution by poplar sawdust. Bioresour. Technol. 99, 2009–2017. https://doi.org/10.1016/j.biortech.2007.03.014.

Pimentel, C.H., Freire, M.S., Gómez-Díaz, D., González-Álvarez, J., 2023. Removal of wood dyes from aqueous solutions by sorption on untreated pine (*Pinus radiata*) sawdust. Cellulose 30, 4587–4608. https://doi.org/10.1007/s10570-023-05145-4.

Przystaś, W., Zabłocka-Godlewska, E., Grabińska-Sota, E., 2012. Biological removal of azo and triphenylmethane dyes and toxicity of process by-products. Water Air Soil Pollut. 223, 1581–1592. https://doi.org/10.1007/s11270-011-0966-7.

Putri, K.N.A., Keereerak, A., Chinpa, W., 2020. Novel cellulose-based biosorbent from lemongrass leaf combined with cellulose acetate for adsorption of crystal violet. Int. J. Biol. Macromol. 156, 762–772. https://doi.org/10.1016/j.ijbiomac.2020.04.100.

Ramisio, P.J., Bento, F., Geraldo, D., Andrade, O., Bettencourt, A.P., 2023. Evaluation of municipal waste compost in relation to the environmental retention of heavy metals. Sustainability 15, 16395. https://doi.org/10.3390/su152316395.

Rios, M.Y., Córdova-Alvores, L.C., Ramírez-Cisneros, M.A., King-Díaz, B., Lotina-Hennsen, B., Rivera, I.L., et al., 2018. Phytotoxic potential of *Zanthoxylum affine* and its major compound linarin as a possible natural herbicide. ACS Omega 3, 14779–14787. https://doi.org/10.1021/acsomega.8b02020.

Saadallah, K., Ad, C., Djedid, M., Benalia, M., Saadallah, S., 2024. Environmental protection by the adsorptive elimination of basic violet 3 dye from water. In: Hamamda, S., Zahaf, A., Sementsov, Y., Nedilko, S., Ivanenko, K. (Eds.), Proceedings of the 2nd International Conference of Nanotechnology for Environmental Protection and Clean Energy Production. Springer Nature, Singapore, pp. 289–296. https://doi.org/10.1007/978-981-97-1916-7_30.

Saeed, A., Sharif, M., Iqbal, M., 2010. Application potential of grapefruit peel as dye sorbent: kinetics, equilibrium and mechanism of crystal violet adsorption. J. Hazard Mater. 179, 564–572. https://doi.org/10.1016/j.jhazmat.2010.03.041.

Sahmoune, M., Yeddou, A.R., 2016. Potential of sawdust materials for the removal of dyes and heavy metals: examination of isotherms and kinetics. Desalination Water Treat. 57, 24019–24034. https://doi.org/10.1080/19443994.2015.1135824.

Sánchez-Martín, J., Beltrán-Heredia, J., Gragera-Carvajal, J., 2011. *Caesalpinia spinosa* and *castanea Sativa* tannins: a new source of biopolymers with adsorbent capacity. Preliminary assessment on cationic dye removal. Ind. Crop. Prod. 34, 1238–1240. https://doi.org/10.1016/j.indcrop.2011.03.024.

Shakoor, S., Nasar, A., 2018. Adsorptive decontamination of synthetic wastewater containing crystal violet dye by employing *Terminalia arjuna* sawdust waste. Groundw. Sustain. Dev. 7, 30–38. https://doi.org/10.1016/j.gsd.2018.03.004.

Sharma, J., Sharma, S., Bhatt, U., Soni, V., 2022. Toxic effects of Rhodamine B on antioxidant system and photosynthesis of *Hydrilla verticillata*. J. Hazard. Mater. Lett. 3, 100069. https://doi.org/10.1016/j.hazl.2022.100069.

Sheppard, M.I., Thibault, D.H., 1992. Desorption and extraction of selected heavy metals from soils. Soil Sci. Soc. Am. J. 56, 415–423. https://doi.org/10.2136/sssaj1992.03615995005600020012x.

Silva, A.C., Rocha, P., Antelo, J., Valderrama, P., López, R., Geraldo, D., et al., 2022a. Comparison of a variety of physico-chemical techniques in the chronological characterization of compost from municipal wastes. Process Saf. Environ. Prot. 164, 781–793. https://doi.org/10.1016/j.psep.2022.06.057.

Silva, A.C., Teixeira, A., Antelo, J., Valderrama, P., Oliveira, R., Cunha, A., et al., 2022b. Distinctive features of composts of different origin: a thorough examination of the characterization results. Sustainability 14, 7449. https://doi.org/10.3390/su14127449.

Skjolding, L.M., Jørgensen, LvG., Dyhr, K.S., Köppl, C.J., McKnight, U.S., Bauer-Gottwein, P., et al., 2021. Assessing the aquatic toxicity and environmental safety of tracer compounds Rhodamine B and Rhodamine WT. Water Res. 197, 117109. https://doi.org/10.1016/j.watres.2021.117109.

Smidt, E., Meissl, K., 2007. The applicability of Fourier transform infrared (FT-IR) spectroscopy in waste management. Waste Manage. (Tucson, Ariz.) 27, 268–276. https://doi.org/10.1016/j.wasman.2006.01.016.

Sudarshan, S., Bharti, V.S., Harikrishnan, S., Shukla, S.P., RathiBhuvaneswari, G., 2022. Eco-toxicological effect of a commercial dye Rhodamine B on freshwater microalgae *Chlorella vulgaris*. Arch. Microbiol. 204, 658. https://doi.org/10.1007/s00203-022-03254-5, 2022.

Thillainayagam, B.P., Saravanan, P., Ravindiran, G., Josephraj, J., 2023. Continuous sorption of methylene blue dye from aqueous solution using effective microorganisms-based water hyacinth waste compost in a packed column. Biomass Conv Bioref 13, 1189–1198. https://doi.org/10.1007/s13399-020-01208-9.

Torrijos, V., Calvo-Dopico, D., Soto, M., 2021. Integration of food waste composting and vegetable gardens in a university campus. J. Clean. Prod. 315, 128175. https://doi.org/10.1016/j.jclepro.2021.128175.

Uddin, F., 2021. Environmental hazard in textile dyeing wastewater from local textile industry. Cellulose 28, 10715–10739. https://doi.org/10.1007/s10570-021-04228-4.

Vigneshpriya, D., Krishnaveni, N., Renganathan, S., 2019. Untreated and *Sargassum* wightii-treated brilliant green dye toxicity impact on microflora and *Allium* cepa L. Appl. Water Sci. 9, 16. https://doi.org/10.1007/s13201-019-0898-8.

Vyavahare, G., Gurav, R., Patil, R., Sutar, S., Jadhav, P., Patil, D., et al., 2021. Sorption of brilliant green dye using soybean straw-derived biochar: characterization, kinetics, thermodynamics and toxicity studies. Environ. Geochem. Health 43, 2913–2926. https://doi.org/10.1007/s10653-020-00804-y.

Witek-Krowiak, A., 2011. Analysis of influence of process conditions on kinetics of malachite green biosorption onto beech sawdust. Chem. Eng. J. 171, 976–985. https://doi.org/10.1016/j.cej.2011.04.048.

Yan, G., Viraraghavan, T., Chen, M.A., 2001. A new model for heavy metal removal in a biosorption column. Adsorpt. Sci. Technol. 19, 25–43. https://doi.org/10.1260/0263617011493953.

Yaseen, G.A., Scholz, M., 2019. Textile dye wastewater characteristics and constituents of synthetic effluents: a critical review. Int. J. Environ. Sci. Technol. 16, 1193–1226. https://doi.org/10.1007/s13762-018-2130-z.

Yu, Y., Murthy, B.N., Shapter, J.G., Constantopoulos, K.T., Voelcker, N.H., Ellis, A.V., 2013. Benzene carboxylic acid derivatized graphene oxide nanosheets on natural zeolites as effective adsorbents for cationic dye removal. J. Hazard Mater. 260, 330–338. https://doi.org/10.1016/j.jhazmat.2013.05.041.